XLI CILAMCE
XLI Ibero-Latin American Congress on Computational Methods in Engineering
16-19 November, 2020 FOZ DO IGUAÇU PARANÁ - BRAZIL

A preliminary study of selected integration methods in XFEM

Jamile M. A. Tavares[1], Erik R. Rodriguez[2], Oscar G. A. de Suarez[2], Rodrigo Rossi[2]

[1]*Depto. de Engenharia Civil, Universidade Federal do Rio Grande do Sul*
Av. João Pessoa, 80, 90040-000, Rio Grande do Sul, Brazil
jamile.tavares@ufrgs.br
[2]*Depto. de Engenharia Mecânica, Universidade Federal do Rio Grande do Sul*
Av. João Pessoa, 80, 90040-000, Rio Grande do Sul, Brazil
erik.rodriguez@ufrgs.br, oagsuarez@gmail.com, rrossi@ufrgs.br

Abstract. In this paper, we conduct a preliminary study of some numerical integration strategies employed in the modeling of weak discontinuity interfaces inside the context of XFEM, such that used as enrichment to model interfaces bi-materials. The first integration strategy considered is the standard Gauss quadrature method. The second uses sub-elements conformed to the discontinuity, which are generated by the Delaunay triangularization. In this case, the Gauss points are applied to the triangular sub-elements and transformed into the quadrilateral element domain. The third technique replaces the discontinuity by an equivalent polynomial that eliminates the use of sub-elements applying directly the standard Gaussian quadrature. A numerical example is carried out in order to draw the very first impressions of the integration strategies.

Keywords: XFEM, weak interfaces, numerical integration.

1 Introduction

The extended finite element method (XFEM) is a partition of unity (PU) based method that allows local extrinsic enrichment of approximation spaces to capture the discontinuities effects caused by interfaces avoiding conforming interface-body meshes and massive adaptive mesh refinement. The standard Gauss quadrature commonly used to numerical integrate the weak form in the finite element method (FEM) works very well for smooth integrands. The same is not true for non-smooth integrands, as the peaks, jumps, and singularities found in the XFEM, severally decreasing the precision of the results Fries and Belytschko [1]. The numerical integration is an important subject of study inside the XFEM, as well as the GFEM.

In Moës, Dolbow, and Belytschko [2], the work recognized to coin the XFEM methodology, but without using the term XFEM, it is called the attention to the necessity of using different strategies to deal with the lack of precision of the standard Gauss quadrature, and it is proposed an integration using sub-elements. The use of sub-elements has proved to be a very efficient technique for the integration of the weak forms in XFEM, especially for static interfaces in linear analysis, having as an advantage not adding degrees of freedom associated with sub-elements.

Fries and Belytschko (2010) proposes an integration procedure with a decomposition of the element into sub-elements aligned with the discontinuity, similar to what is the standard in FEM. According to Natarajan, Mahapatra, and Bordas [3] and Seabra *et al.* [4], this decomposition of the elements is the conventional one in XFEM, but these authors use this type of integration only to compare their results which are obtained using different strategies. This type of integration is used by Kästner *et al.* [5] and also by Béchet *et al.* [6] so that the integrated functions are continuous in each sub-element. Ventura [7] states that this is a common technique, but seeks for a method so that it is not needed.

Ventura [7] employs the standard Gauss quadrature in the discontinuous elements without decompose the element or introducing any approximation. The technique used is based on the analysis of the element stiffness. Based on the nodal value of the level set, it is shown that there is an equivalent polynomial, whose integration provides exactly the value of the integrated function in the sub-element. Such a polynomial is defined in the element domain, so it can be integrated by the standard Gaussian square.

In the present work, the standard Gauss quadrature, the integration with triangular sub-elements, and integration with equivalent polynomials were used in a simple example with a weak discontinuity in order to assess the differences in the precision of such integration strategies, taking as the reference numerical solution that obtained using sub-elements.

This work is organized in four sections. This introduction, section 2 where it is shortly described the main aspects of the integration with triangular sub-elements and the integration using equivalent polynomials. The numerical results are presented in section 3 and section 4 our conclusions.

2 Numerical integration in XFEM

The approximation field in XFEM can be written as

$$\mathbf{u}(\mathbf{x}) = \sum_{i=1}^{n} N_i(\mathbf{x})\bar{\mathbf{u}}_i + \sum_{j=1}^{m} N_j^*(\mathbf{x})\varphi(\mathbf{x})\bar{\mathbf{a}}_j \tag{1}$$

where $\mathbf{u}(\mathbf{x})$ is the displacement vector, n is the set of nodal points, $N_i(\mathbf{x})$ are the standard FEM shape functions, $N_j^*(\mathbf{x})$ are the enrichment shape function, $\bar{\mathbf{u}}_i$ is the degree of freedom associated with the standard FEM shape function, $\bar{\mathbf{a}}_j$ is the degree of freedom associated with the enrichment function, $\varphi(\mathbf{x})$ is the so called *enrichment function*, and m is the number of enriched nodes.

For weak discontinuities, discontinuities related to bi-material interfaces in the domain, enrichment functions are used through the Level Set method (LSM), Pathak, A. Singh, and I. Singh [8]. The Level set Method is used to represent the interface geometry implicitly. This method represents the interface by an implicit function in the domain, in this way the interface is defined as the zero of the function and having one dimension less than the geometric domain.

Let Ω by a domain divided by an interface Γ_d into the subdomains Ω_A and Ω_B. The level set function used is the so-called signed-distance function, which is defined by the representation of the interface position, according to

$$\varphi(\mathbf{x}) = \min_{\mathbf{x}^* \in \Gamma_d} \left\| \mathbf{x} - \mathbf{x}^* \right\| \text{sign}(\mathbf{n}_{\Gamma_d} \cdot (\mathbf{x} - \mathbf{x}^*)) \tag{2}$$

where $\mathbf{x} \in \Omega$, $\mathbf{x}^*$ is a point on the interface defined as the orthogonal projection of $\mathbf{x}$ to the interface Γ_d, $\mathbf{n}_{\Gamma_d}$ is the normal vector to the interface Γ_d, and $\left\| \mathbf{x} - \mathbf{x}^* \right\|$ is the distance from $\mathbf{x}$ to $\mathbf{x}^*$ given by the Euclidian norm, that is, the distance from $\mathbf{x}$ to the interface.

2.1 Integration by triangular sub-elements

The triangularization of elements crossed by a discontinuity is one of the most used rules in XFEM. It consists of dividing the element into small triangles and applying the Gauss rules within the sub-element. The triangular sub-elements are easily obtained for convex regions using the Delaunay triangularization.

In order to avoid a massive use of sub-elements, and then improve the inputs to the Delaunay triangularization algorithm, one can work with few sub-elements but augment the number of integration points, although it is reported that the computation cost is higher for the last case to achieve the same level of precision in comparison to the use of more sub-elements [4].

Given an element with a crossing interface, what is the case of interest of this study, the division into triangular sub-elements follows as presented in Fig. 1. Given the Delaunay triangularization knowing each sub-triangle coordinate vertex $\mathbf{x}_i$ at the Cartesian plane (x, y) and knowing the Gauss integration quadrature in the parametric system (r, s), the coordinates of the integrations points can be easily determined in the Cartesian plane by the use of the shape functions of the triangular element, also known as the Constant Strain Triangle (CST), by

$$\begin{aligned} x &= (x_2 - x_1)r + (x_3 - x_1)s + x_1. \\ y &= (y_2 - y_1)r + (y_3 - y_1)s + y_1. \end{aligned} \tag{3}$$

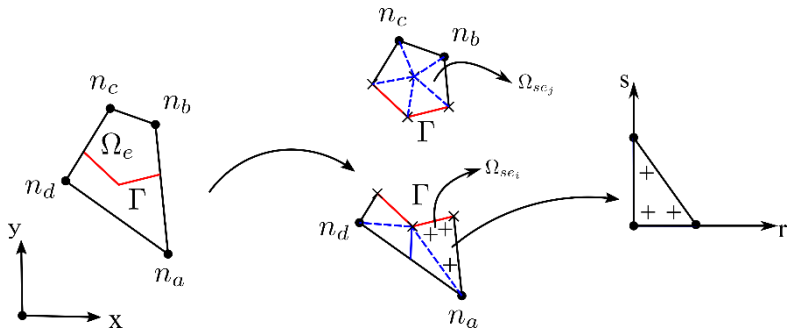

Figure 1. Decomposition of a quadrilateral element crossed by and interface in triangular sub-elements.

The Jacobian Matrix of such transformation is given by

$$J_{sub-e} = \frac{\partial(x,y)}{\partial(r,s)} = \begin{pmatrix} \frac{\partial x}{\partial r} & \frac{\partial y}{\partial r} \\ \frac{\partial x}{\partial s} & \frac{\partial y}{\partial s} \end{pmatrix} \rightarrow J_{sub-e} = \begin{pmatrix} (x_2 - x_1) & (y_2 - y_1) \\ (x_3 - x_1) & (y_3 - y_1) \end{pmatrix}. \tag{4}$$

Once the integration points in the Cartesian plane were known, it was necessary to transform these points for the parametric system (ξ, η) of the quadrilateral element. The mapping from local coordinates (ξ, η) to the Cartesian plane (x, y) follows the equation

$$\mathbf{x} = \sum_i N_i(\xi, \eta)\, x_i \,. \tag{5}$$

The inverse of this mapping, $(x, y) \rightarrow (\xi, \eta)$, is not simple because it involves a nonlinear system of equations that cannot be obtained analytically, so a numerical approximation is necessary. There are several ways to solve this problem. In this paper, we have implemented the method proposed by Murti and Valliappan [9].

In Murti and Valliappan [9] the iteration procedure to determine the inverse mapping has been improved by the intersection of a defined line that passes through a point M, defined at the interior of the element, whose Cartesian coordinates are $\mathbf{x}_m$, and a point P whose the local parametric coordinate ξ_p is known, such that a node of the vertex of the element.

For this characterization, the point M is assumed to be the Gauss point that need to be determined in terms of the parametric coordinates ξ_m, corresponding to the point M' in Fig. 2.

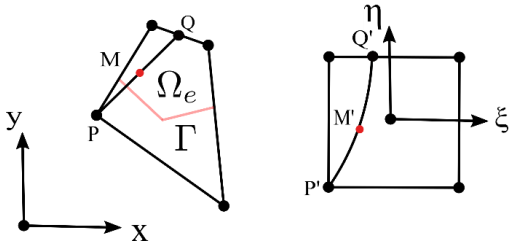

Figure 2. The schematization of the method proposed by Murti and Valliappan [9].

The segment $\overline{PQ}$ in the Cartesian plane can be easily determined by the linear equation of the line passing by the points P and M. This segment is associated with the curve $P'Q'$ on the local coordinate plane and passing through the point M'. Thus, the coordinate of the point M', ξ_m, can be determined more efficiently when compared to a numerical method without any improvement condition.

To determine the point M' on the curve $P'Q'$ the false position method was employed, Lim *et al.* [10]. In Murti and Valliappan [9] the authors have used the bisection method, but the number of iterations for this method was higher.

The point P cannot be any vertex of the element. It must be chosen so that the curve $P'Q'$ be defined in the element, that is, it must cover the entire axis η at the interval $[-1, +1]$. In the present work, when this occurs,

the point P is redefined as the vertex opposite to the previous one, while in Murti and Valliappan [9] the authors choose to renumber the element nodes, so there is a transformation of the axis η to ξ.

Mathematically, the first step was to determine the line containing the segment $\overline{PQ}$, that is

$$\overline{PQ} \equiv y = ax + c \,. \tag{6}$$

in which $a = \left(y_m - y_p\right)/\left(x_m - x_p\right)$ and $c = y_p - ax_p$. Rearranging eq. (6) yields

$$N_i y_i = a(N_i x_i) + c \,. \tag{7}$$

Or, as the system

$$\begin{matrix} N_i (y_i - ax_i) - c = 0 \\ N_i \gamma_i - c = 0 \end{matrix} \,. \tag{8}$$

As γ_i and c are constants for the points M and P, eq. (8) can be reorganized accordingly to

$$A\xi^2 + B\xi + C = 0 \,. \tag{9}$$

The coefficients A, B, and C are functions of (γ_i, η, c). Therefore, these coefficients vary with the number of the nodes of the quadrilateral element. For the quadrilateral element of 4 nodes such coefficients are.

$$A = 0 \,. \tag{10}$$

$$B = \frac{1}{4}\left(\left(\gamma 2 - \gamma 1\right)\left(1 - \eta\right) + \left(\gamma 3 - \gamma 4\right)\left(1 + \eta\right)\right) \,. \tag{11}$$

$$C = \frac{1}{4}\left(-\left(\gamma 1 + \gamma 2\right)\left(-1 + \eta\right) + \left(\gamma 3 + \gamma 4\right)\left(1 + \eta\right)\right) - c \,. \tag{12}$$

Only one root of the eq. (9) is the solution. It is determined when, at the iteration n, one gets satisfied for the tolerance δ_n:

$$\delta_n \geq \mathbf{x}_m - N_i(\xi_m^n) \,. \tag{13}$$

Once the integration points are obtained on the parametric system (ξ, η) The stiffness matrix can be integrated into each triangular sub-element using.

$$\mathbf{K}_{sub-e} = \int_{\Omega \text{ sub-e}} \det[J_{sub-e}]\mathbf{[B]}^{\mathbf{T}}\mathbf{[D][B]}d\Omega \simeq \sum_{i=1}^{n} w_i \det[J_{sub-e}]\mathbf{[B]}^{\mathbf{T}}\mathbf{[D][B]} \,. \tag{14}$$

where n is the number of integration points, w_i is weight. The matrices **[B]** and **[D]** are depending on the variables ξ and η, and are integrated at the points (ξ_i, η_i), which are the Gauss points of the triangular sub-element transformed to this coordinate system.

The element stiffness matrix $\mathbf{K}_e$ is the sum of the sub-elements stiffness matrices $\mathbf{K}_{sub-e}$, that is,

$$\mathbf{K}_e = \sum_{sub=1}^{nk} \mathbf{K}_{sub-e} \,. \tag{15}$$

where nk is the total number of the sub-elements of the element e.

2.2 Integration by equivalent polynomials.

Let us rewrite eq. (1) as

$$\mathbf{u}(\mathbf{x}) = \sum_{i=1}^{n} N_i(\mathbf{x})\bar{\mathbf{u}}_i + \sum_{j=1}^{m} N_j(\mathbf{x})\left|\varphi(\mathbf{x})\right|\bar{\mathbf{a}}_j \,. \tag{16}$$

where $|\varphi(\mathbf{x})|$ is the signed distance function.

In the matrix format with f_e denoting the enrichment function

$$\mathbf{u} = \mathbf{N}\mathbf{u}_\mathbf{e} + \mathbf{N}f_e\mathbf{a}_\mathbf{e}\,. \tag{17}$$

The enrichment function $\varphi(\mathbf{x})$ is the *Level Set* function, and the displacement becomes

$$\mathbf{u} = \mathbf{N}\mathbf{u}_\mathbf{e} + |\varphi(\mathbf{x})|\,\mathbf{N}\mathbf{a}_\mathbf{e} - \mathbf{N}(|\varphi(\mathbf{x}_j)|\,\mathbf{I})\mathbf{a}_\mathbf{e} \tag{18}$$

in which $|\varphi(\mathbf{x}_j)|\,\mathbf{I}$ is the Level Set function at the nodes of the elements and **I** the identity matrix.

The strain field as the following format

$$\boldsymbol{\varepsilon} = \mathbf{B}\mathbf{u}_\mathbf{e} + |\varphi(\mathbf{x})|\,\mathbf{B}\mathbf{a}_\mathbf{e} + (\nabla_\varepsilon\,|\varphi(\mathbf{x})|)\mathbf{N}\mathbf{a}_\mathbf{e} - \mathbf{B}(|\varphi(\mathbf{x}_j)|\,\mathbf{I})\mathbf{a}_\mathbf{e}\,, \tag{19}$$

and the stress can be computed, for linear elastic isotropic materials, using the constitutive relation $\boldsymbol{\sigma} = \mathbf{E}\boldsymbol{\varepsilon}$. The internal virtual work of an element is determined by

$$L_i = \int_{\Omega_e} \boldsymbol{\varepsilon}^{\mathrm{T}}\boldsymbol{\sigma}\mathrm{d}\Omega = \int_{\Omega_e} \boldsymbol{\varepsilon}^{\mathrm{T}}\mathbf{E}\boldsymbol{\varepsilon}\mathrm{d}\Omega\,. \tag{20}$$

By introducing eq. (19) in eq. (20) one writes

$$L_i = \int_{\Omega_e} (\mathbf{u_e}^T\mathbf{B}^T + \mathbf{a_e}^T H\varphi\mathbf{B}^T + \mathbf{a_e}^{\mathrm{T}}\mathbf{N}^{\mathrm{T}}(H\mathfrak{E})^{\mathrm{T}} - (\mathbf{a_e}^{\mathrm{T}}(\mathfrak{F})^{\mathrm{T}}\mathbf{B}^{\mathrm{T}}))\mathbf{E}(\mathbf{B}\mathbf{u}_\mathbf{e} + H\varphi\mathbf{B}\mathbf{a}_\mathbf{e} + (H\mathfrak{E})\mathbf{N}\mathbf{a}_\mathbf{e} - \mathbf{B}(\mathfrak{F})\mathbf{a}_\mathbf{e})\mathrm{d}\Omega\,. \tag{21}$$

in which, we have used the following notation to simplify the writing: $|\varphi(\mathbf{x})|$ by $H\varphi$, $\nabla_\varepsilon\,|\varphi(\mathbf{x})|$ by $H\mathfrak{E}$ and $|\varphi(\mathbf{x}_j)|\,\mathbf{I}$ by the symbol $\mathfrak{F}$. Expanding eq. (21) one gets the stiffness matrix

$$K_e = \int_{\Omega_e}\begin{bmatrix} \mathbf{B}^T\mathbf{E}\mathbf{B} & 0 \\ (H\varphi)\mathbf{B}^T\mathbf{E}\mathbf{B} + \mathbf{N}^{\mathrm{T}}(H\mathfrak{E})^{\mathrm{T}}\mathbf{E}\mathbf{B} - (H\mathfrak{F})^{\mathrm{T}}\mathbf{B}^{\mathrm{T}}\mathbf{E}\mathbf{B} & 0 \end{bmatrix}\mathrm{d}\Omega + \int_{\Omega_e}\begin{bmatrix} 0 & \mathbf{B}^T\mathbf{E}(H\varphi)\mathbf{B} + \mathbf{B}^T\mathbf{E}(H\mathfrak{E})\mathbf{N} - \mathbf{B}^T\mathbf{E}\mathbf{B}(\mathfrak{F}) \\ 0 & \begin{array}{l} H\varphi\mathbf{B}^T\mathbf{E}(H\varphi)\mathbf{B} + \mathbf{N}^{\mathrm{T}}(H\mathfrak{E})^{\mathrm{T}}\mathbf{E}(H\varphi)\mathbf{B} + H\varphi\mathbf{B}^T\mathbf{E}(H\mathfrak{E})\mathbf{N} + \mathbf{N}^{\mathrm{T}}(H\mathfrak{E})^{\mathrm{T}}\mathbf{E}(H\mathfrak{E})\mathbf{N} + (\mathfrak{F})^{\mathrm{T}}\mathbf{B}^{\mathrm{T}}\mathbf{E}\mathbf{B}(\mathfrak{F}) \\ -H\varphi\mathbf{B}^T\mathbf{E}\mathbf{B}(\mathfrak{F}) - \mathbf{N}^{\mathrm{T}}(H\mathfrak{E})^{\mathrm{T}}\mathbf{E}\mathbf{B}(\mathfrak{F}) - (\mathfrak{F})^{\mathrm{T}}\mathbf{B}^{\mathrm{T}}\mathbf{E}(H\varphi)\mathbf{B} - (\mathfrak{F})^{\mathrm{T}}\mathbf{B}^{\mathrm{T}}\mathbf{E}(H\mathfrak{E})\mathbf{N} \end{array} \end{bmatrix}\mathrm{d}\Omega. \tag{22}$$

The constitutive matrix for a bi-material body can be written as

$$\mathbf{E} = \mathbf{E_m} + H(\mathbf{x})\Delta\mathbf{E}\,. \tag{23}$$

in which $\mathbf{E_m} = \frac{1}{2}(\mathbf{E1} + \mathbf{E2})$ and $\Delta\mathbf{E} = \frac{1}{2}(\mathbf{E1} - \mathbf{E2})$. By substituting eq. (23) in eq. (22) it is possible to write the element stiffness matrix K_e as the contribution of two parts.

The special functions are separated in two categories, continuous and continuous by parts in Tab. 1.

Table 1. Continuity of integration functions for material discontinuity

Continuous and differentiable	Continuous and differentiable by parts
H^2	H
φ	$H\varphi$
φ^2	H^3
$H^2\varphi$	$H^3\varphi$
$H^2\varphi^2$	$H^3\varphi^2$

Replacing the equivalent polynomials $\tilde{H}$ by Heaviside function H and $\tilde{Q}$ by the ramp function module, $H\varphi$, in the discontinuous, the stiffness matrix is obtained with continuous terms

$$
\begin{aligned}
K_e = & \int_{\Omega_e} \begin{bmatrix} \mathbf{B}^T\mathbf{E}_\mathbf{m}\mathbf{B} & 0 \\ H^2\varphi\mathbf{B}^T\Delta\mathbf{E}\mathbf{B} + H^2\mathbf{N}^{\mathrm{T}}\mathfrak{E}^{\mathrm{T}}\Delta\mathbf{E}\mathbf{B} - \mathfrak{F}^{\mathrm{T}}\mathbf{B}^{\mathrm{T}}\mathbf{E}_\mathbf{m}\mathbf{B} & 0 \end{bmatrix} \mathrm{d}\Omega + \\
& \int_{\Omega_e} \begin{bmatrix} 0 & H^2\varphi\mathbf{B}^T\Delta\mathbf{E}\mathbf{B} + H^2\mathbf{B}^T\Delta\mathbf{E}\mathfrak{E}\mathbf{N} - \mathbf{B}^T\mathbf{E}_\mathbf{m}\mathbf{B}\mathfrak{F} \\ 0 & H^2\varphi^2\mathbf{B}^T\mathbf{E}_\mathbf{m}\mathbf{B} + H^2\varphi\mathbf{N}^{\mathrm{T}}\mathfrak{E}^{\mathrm{T}}\mathbf{E}_\mathbf{m}\mathbf{B} + H^2\varphi\mathbf{B}^T\mathbf{E}_\mathbf{m}\mathfrak{E}\mathbf{N} + H^2\mathbf{N}^{\mathrm{T}}\mathfrak{E}^{\mathrm{T}}\mathbf{E}_\mathbf{m}\mathfrak{E}\mathbf{N} + \mathfrak{F}^{\mathrm{T}}\mathbf{B}^{\mathrm{T}}\mathbf{E}_\mathbf{m}\mathbf{B}\mathfrak{F} \\ & -H^2\varphi\mathbf{B}^T\Delta\mathbf{E}\mathbf{B}\mathfrak{F} - H^2\mathbf{N}^{\mathrm{T}}\mathfrak{E}^{\mathrm{T}}\Delta\mathbf{E}\mathbf{B}\mathfrak{F} - H^2\varphi\mathfrak{F}^{\mathrm{T}}\mathbf{B}^{\mathrm{T}}\Delta\mathbf{E}\mathbf{B} - H^2\mathfrak{F}^{\mathrm{T}}\mathbf{B}^{\mathrm{T}}\Delta\mathbf{E}\mathfrak{E}\mathbf{N} \end{bmatrix} \mathrm{d}\Omega + \\
& \int_{\Omega_e} \begin{bmatrix} \tilde{H}\mathbf{B}^T\Delta\mathbf{E}\mathbf{B} & 0 \\ \tilde{Q}\mathbf{B}^T\mathbf{E}_\mathbf{m}\mathbf{B} + \tilde{H}\mathbf{N}^{\mathrm{T}}\mathfrak{E}^{\mathrm{T}}\mathbf{E}_\mathbf{m}\mathbf{B} - \tilde{H}\mathfrak{F}^{\mathrm{T}}\mathbf{B}^{\mathrm{T}}\Delta\mathbf{E}\mathbf{B} & 0 \end{bmatrix} \mathrm{d}\Omega + \\
& \int_{\Omega_e} \begin{bmatrix} 0 & \tilde{Q}\mathbf{B}^T\mathbf{E}_\mathbf{m}\mathbf{B} + \tilde{H}\mathbf{B}^T\mathbf{E}_\mathbf{m}\mathfrak{E}\mathbf{N} - \tilde{H}\mathbf{B}^T\Delta\mathbf{E}\mathbf{B}\mathfrak{F} \\ 0 & \tilde{H}H^2\varphi^2\mathbf{B}^T\Delta\mathbf{E}\mathbf{B} + H^2\tilde{Q}\mathbf{N}^{\mathrm{T}}\mathfrak{E}^{\mathrm{T}}\Delta\mathbf{E}\mathbf{B} + H^2\tilde{Q}\mathbf{B}^T\Delta\mathbf{E}\mathfrak{E}\mathbf{N} + \tilde{H}H^2\mathbf{N}^{\mathrm{T}}\mathfrak{E}^{\mathrm{T}}\Delta\mathbf{E}\mathfrak{E}\mathbf{N} + \tilde{H}\mathfrak{F}^{\mathrm{T}}\mathbf{B}^{\mathrm{T}}\Delta\mathbf{E}\mathbf{B}\mathfrak{F} \\ & -\tilde{Q}\mathbf{B}^T\mathbf{E}_\mathbf{m}\mathbf{B}\mathfrak{F} - \tilde{H}\mathbf{N}^{\mathrm{T}}\mathfrak{E}^{\mathrm{T}}\mathbf{E}_\mathbf{m}\mathbf{B}\mathfrak{F} - \tilde{Q}\mathfrak{F}^{\mathrm{T}}\mathbf{B}^{\mathrm{T}}\mathbf{E}_\mathbf{m}\mathbf{B} - \tilde{H}\mathfrak{F}^{\mathrm{T}}\mathbf{B}^{\mathrm{T}}\mathbf{E}_\mathbf{m}\mathfrak{E}\mathbf{N} \end{bmatrix} \mathrm{d}\Omega.
\end{aligned}
\tag{24}
$$

The procedure for calculating the polynomials and their coefficients is found in the work of Ventura [7], as well as the used distance function used which is based on the shape functions. Such function, for the bilinear quadrilateral element, is given by

$$\varphi(\xi,\eta) = \frac{1}{2}[(1+\xi)d_2 + (1+\eta)d_4 - (\eta+\xi)d_1]. \tag{25}$$

where d_1, d_2, and d_4 are the distances from the discontinuity line to the nodes of the element.

3 Numerical results

In order to establish a comparison between the different types of integration presented here, it was decided to use the result of the integration with the sub-element technique as the reference solution and then to compare the standard Gaussian integration with the integration with equivalent polynomials. For this, the model problem of a Bi-material bar under tension modeled by plane elements with an interface, see Fig. 3. The dimensions are L=20cm, Young modulus E=2x10^6 kg/cm², Poisson ratio v=0.3, for the material to the left of the interface and 0.5E and v for the material to the right, the tensile load q=2x10^4 kg/cm. This figure also shows the tilt in the interface used to assess the capacity of the integration of each method.

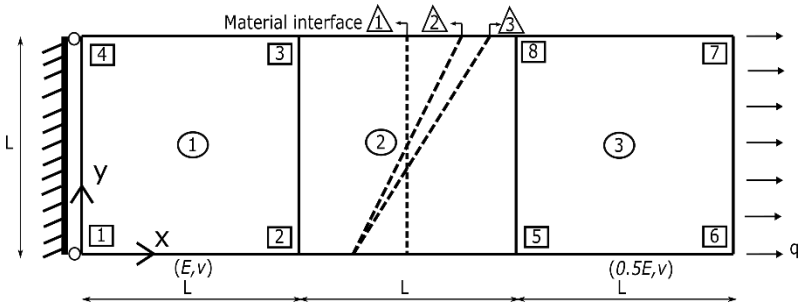

Figure 3. Bi-material bar under tension modeled by plane elements with an interface.

The material interface 1 has coordinates (30,-10) and (30,10), the interface 2 (25,-10) and (35,-10), and the interface 3 (25,-10) and (37.5, 10). This problem with material interface 1 is presented in Khoei [11].

The displacements were calculated for each of the integration techniques, and then the relative errors as

$$e = \left| \frac{u_{i-subelemento} - u_i}{u_{i-subelemento}} \right|. \tag{26}$$

where $u_{i-subelemento}$ is the displacement obtained with the integration by triangular sub-elements, u_i is (in turns) the displacement obtained by the standard Gauss method and by the method with equivalent polynomials.

The compared displacements correspond to the largest displacement that occurs in the structure, horizontal of the node 6, that is, u_{6_y}. In the standard Gauss integration and in the integration with equivalent polynomials, 16 Gauss points were used, while in the integration with sub-elements 8 triangular sub-elements with 6 Gauss points each were used. Tab. 2 shows the relative errors for each case.

Table 2. Quadrature error for standard method and equivalent polynomial for the u_{6_y} .

interface	Gauss standard	Equivalent polynomial
1	0.13	0.00
2	0.27	0.27
3	1.08	0.53

4 Conclusions

Three numerical integration techniques were used and compared. From the results obtained, integration with equivalent polynomials showed the smallest error compared to the standard Gaussian quadrature. Integration with triangular sub-elements was used as a reference because it is the most commonly used integration in XFEM. However, it is necessary to continue research and implement integration with equivalent polynomials for distorted elements.

Acknowledgements. The support of the Federal University of Rio Grande do Sul, PPGEC, GMAp, CNPq, and FAPERGS for financial research support. Grant numbers: CNPq 306058/2018-9, FAPERGS: 19/2551-0001954-8-1.

Authorship statement. The authors hereby confirm that they are the sole liable persons responsible for the authorship of this work, and that all material that has been herein included as part of the present paper is either the property (and authorship) of the authors, or has the permission of the owners to be included here.

References

[1] T. P. Fries and T. Belytschko, "The extended/generalized finite element method: An overview of the method and its applications," *International Journal for Numerical Methods in Engineering*, p. 253–304, 23 April 2010.
[2] N. Moës, J. Dolbow and T. Belytschko, "A Finite Element Method for Crack Growth without Remeshing," *International Journal for Numerical Methods in Engineering*, pp. 131-150, 1999.
[3] S. Natarajan, D. R. Mahapatra and S. P. A. Bordas, "Integrating strong and weak discontinuities without integration subcells and example applications in an XFEM/GFEM framework," *International Journal for Numerical Methods in Engineering*, pp. 269-294, 29 January 2010.
[4] M. R. R. Seabra, J. M. A. C. d. Sa, P. Šuštarič and T. Rodič, "Some numerical issues on the use of XFEM for ductile fracture," *Computational Mechanics*, p. 611–629, 11 March 2012.
[5] M. Kästner, S. Müller, J. Goldmann, C. Spieler, J. Brummund and V. Ulbricht, "Higher-order extended FEM for weak discontinuities – level set representation, quadrature and application to magneto-mechanical problems," *International Journal for Numerical Methods in Engineering*, p. 1403–1424, 19 December 2012.
[6] E. Béchet, H. Minnebo, N. Moës and B. Burgardt, "Improved implementation and robustness study of the X-FEM for stress analysis around cracks," *International Journal for Numerical Methods in Engineering*, pp. 1033-1056, june 2005.
[7] G. Ventura, "On the elimination of quadrature subcells for discontinuous functions in the eXtended Finite-Element Method," *International Journal for Numerical Methods in Engineering*, p. 761–795, 12 December 2005.
[8] H. Pathak, A. Singh and I. V. Singh, "Numerical simulation of bi-material interfacial cracks using EFGM and XFEM," *International Journal of Mechanics and Materials in Design*, pp. 9-36, 2011.
[9] V. Murti and S. Valliappan, "Numerical inverse isoparametric mapping in remeshing and nodal quantity contouring," *Computer & Structures*, pp. 1011-1021, 1985.
[10] I. L. Lim, I. W. Johnston, S. K. Choi e V. Murti, "An improved numerical inverse isoparametric mapping technique for 2D mesh rezoning," *Engineering Fracture Mechanics*, vol. 41, pp. 417-435, 1992.
[11] A. R. Khoei, *Extended Finite Element Method: Theory and Applications*, Wiley, 2015.